Proceedings of the 2007 American Control Conference
Marriott Marquis Hotel at Times Square
New York City, USA, July 11-13, 2007

Modeling and Distributed Control of an Electrostatically Actuated Microcantilever Array

Azeem Sarwar, Petros G. Voulgaris, and Srinivasa M. Salapaka

Abstract— **This paper presents a basic model and control design of an array of electrostatically actuated microcantilevers that can be put to use for high throughput applications, such as, multi cantilever imaging applications in Atomic Force Microscopy (AFM). We consider a model of infinite array which belongs to the class of spatially invariant systems, and design a $\mathscr{H}_\infty$ distributed controller while making use of the information from only the immediate neighbors. The performance of this controller is tested via simulations on a finite nonlinear model of the system. Based on the achieved resolution and bandwidth, the device holds high potential for AFM applications in contact mode such as, indenting, pushing, cutting, and lithography.**

I. INTRODUCTION

The integration of sensors and actuators, and the use of array architectures in the scanning probe microscopy have resulted in the use of piezoresistive [1], [2], piezolectric [3], [4], [6], thermal expansion [7] or capacitive effects [8], [9]. The parallelism together with miniaturization normally introduces dynamic coupling between the individual elements. The current practice to eliminate the coupling effects is to introduce large spacing amongst the individual elements. This practice essentially reduces the dynamic coupling effects, however, it compromises on the throughput of the device. Hence, a revolutionary step in the field of nano-technology calls for the development of a control scheme that can successfully allow independent actuation without compromising the miniaturization, and therefore the device throughput.

With this motivation in mind we attempt to efficiently address the coupling problem without compromising the throughput of the device in question. In particular, we consider a system of very closely spaced microcantilevers that can be capacitively actuated and sensed independently. A major advantage of the capacitive detection is the fact that it offers both electrostatic actuation as well as integrated detection. The basic dynamical model for a pair of cantilevers derived from [10] is extended for the case of an infinite array of cantilevers that is used to represent a suitable model of the heavily packed array. Such a model belongs to the class of spatially invariant systems, which means that there exists a notion of translation in some spatial coordinates, with respect to which the system's dynamics are invariant. This allows the effective application of recently developed [13] control techniques that make use of the system's spatially invariant structure yielding a distributed infinite array of finite dimensional controllers. The effectiveness of these techniques is demonstrated in simulation of the nonlinear model of a finite array.

The paper is organized as follows: Modeling and description of the system is presented in Section II. Section III presents a distributed controller architecture for the problem in question. Finally, we conclude our discussion in Section IV.

II. SYSTEM MODELING AND DESCRIPTION

The system consists of infinitely many microcantilevers connected to the same base, each forming a micro-capacitor, with the second rigid plate located underneath the cantilever. The cantilever is flexible and can move in the vertical axis, however it is assumed to be rigid along the horizontal axis. The vertical displacement of each cantilever can be controlled by applying voltage across the plates. Although each cantilever is independently actuated, its dynamics are influenced by the presence of other cantilevers. This coupling is of two types; 1) mechanical, since the microcantilevers are attached to the same base 2) electrical, due to the fringing fields generated by the capacitors nearby. The force acting on each microcantilever can be split in its components along the three axes. Since the microcantilevers are assumed to be non rigid only along the vertical axis, the equation of motion only for the vertical displacement z_i is considered. For $i \in \mathbb{Z}$ (integers), we can write the equation of motion of each microcantilevers as

$$\ddot{z}_i + b\dot{z}_i + \omega^2 z_i = F_{a,i} + F_{mech,i} + F^{\perp}_{elec,i} \tag{1}$$

where b is the normalized damping coefficient [11]. ω is the natural resonant frequency of the i_{th} microcantilever beam [10]. $F_{a,i}$ is the attractive force between the capacitor plates of the i_{th} microcantilever and is given by the following expression

$$F_{a,i} = \frac{\varepsilon_0 A}{2md^2}(1 + \frac{2z_i}{d})U_i^2$$

where ε_0 is the permittivity in vacuum, d in the above expression is the gap between the electrodes, A is area of the capacitor plates, m mass, and U_i is the voltage applied. $F_{mech,i}$ is an equivalent mechanical coupling force exerted on the i_{th} microcantilever by its neighbors and is given by the following expression

$$F_{mech,i} = \frac{1}{m}\sum_{j=i-1, j\neq i}^{i+1} \gamma_{i,j}(z_j - z_i) \tag{2}$$

where $\gamma_{i,i+1}$ is the coefficient of mechanical coupling [12]. $F^{\perp}_{elec,i}$ is the electrostatic coupling force exerted on the i_{th} microcantilever beam by its neighbors and is given by the following expression

$$F^{\perp}_{elec,i} = \frac{c_i U_i}{m4\pi\varepsilon_0}\sum_{j=-\infty, j\neq i}^{\infty} \frac{c_j U_j (z_i - z_j)}{r_{i,j}^3} \tag{3}$$

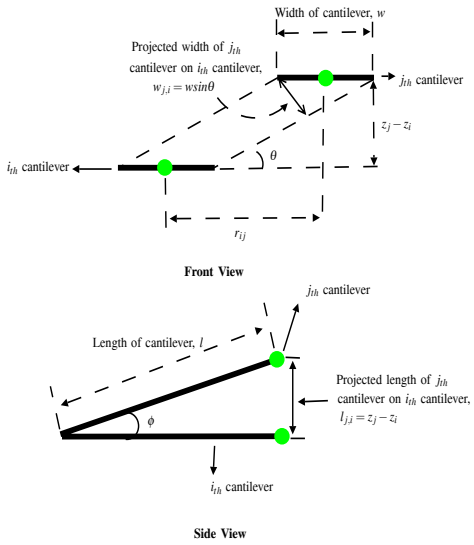

Fig. 1. Projected Area of j_{th} Cantilever on i_{th} Cantilever

where c_i, and c_j is the capacitance of the i_{th} and j_{th} microcantilever respectively, U_i, and U_j is the voltage applied across the i_{th} and j_{th} microcantilever respectively, and $r_{i,j}$ is the horizontal distance between the centroids of i_{th} and j_{th} microcantilever.

A. Mechanical and Electrostatic Coupling

The mechanical coupling has been modeled as a spring like force, proportional to the difference in the vertical displacement z_i of the cantilevers.

Following the lines of [10], the voltage applied to each capacitor was considered to be inducing charge on its neighbors, specifically the following expression was considered for the charge on the i_{th} plate.

$$q_i = c_i U_i + \sum_{j=-\infty, j\neq i}^{\infty} c_{i,j} U_{i,j}; \text{ where } c_i = \varepsilon_0 \frac{A}{d - z_i}$$

Using the parallel plate capacitor theory the expression of $c_{i,j}$ is given as $c_{i,j} = \varepsilon_0 \frac{A_{i,j}}{d_{i,j}}$ where $A_{i,j}$ is the projected area of j_{th} microcantilever onto the i_{th} microcantilever and $d_{i,j}$ is the displacement between the centroid of the i_{th} and the j_{th} microcantilever. Referring to the Figure 1 the area projected by j_{th} microcantilever on the i_{th} cantilever is, given by the following expression

$$A_{i,j} = w_{i,j} \times l_{i,j} = w \frac{(z_j - z_i)^2}{\sqrt{r_{i,j}^2 + (z_i - z_j)^2}}$$

The corresponding expression for the capacitance $c_{i,j}$, is therefore given as follows

$$c_{j,i} = \varepsilon_0 \frac{w(z_j - z_i)^2}{r_{i,j}^2 + (z_i - z_j)^2}$$

The charge induced by the neighboring cantilevers asymptotes quite rapidly as we move away from the reference microcantilever owing to the presence of the term $r_{j,i}^2$ in the denominator of the expression of $c_{j,i}$. It was also noticed that the contribution of charge induced by the neighbors on the reference cantilever is insignificant, and hence the expression, $\sum_{j=-\infty, j\neq i}^{\infty} c_{i,j} U_{i,j}$ was neglected in rest of the analysis.

The charges induced on each microcantilever results in an electrostatic interaction amongst the microcantilevers. As in [10], the interaction between these induced charges is described via a point charge model. Each microcantilever is represented as a charged particle, q_i, and the mutual interaction is described by the Coulombs law

$$F_{elec,i} = \frac{c_i U_i}{4\pi\varepsilon_0} \sum_{j=-\infty, j\neq i}^{\infty} \frac{c_j U_j}{r_{i,j}^2}$$

and the vertical component of this force is given as

$$\begin{aligned} F_{elec,i}^{\perp} = & \frac{c_i U_i}{4\pi\varepsilon_0} \sum_{j=-\infty, j\neq i}^{\infty} \frac{c_j U_j (z_i - z_j)}{r_{i,j}^2 \sqrt{r_{i,j}^2 + (z_i - z_j)^2}} \\ \approx & \frac{c_i U_i}{4\pi\varepsilon_0} \sum_{j=-\infty, j\neq i}^{\infty} \frac{c_j U_j (z_i - z_j)}{r_{i,j}^3} \end{aligned}$$

since $(z_i - z_j)^2 \approx 0$. Clearly $F_{elec,i}^{\perp} \rightarrow$constant, as $r_{i,j} \rightarrow \infty$.

B. Spatial Invariance

The system can be treated as being spatially invariant in nature since the same dynamical model holds for each microcantilever and hence the generalized equation of motion, for the i_{th} cantilever can be given as follows

$$\begin{aligned} \ddot{z}_i + b\dot{z}_i + \omega^2 z_i = & \frac{\varepsilon_o A}{2md^2}\left(1 + \frac{2z_i}{d}\right) U_i^2 + \frac{1}{m} \sum_{j=i-1, \neq i}^{j=i+1} \gamma_{i,j}(z_j - z_i) \\ & + \frac{c_{i,i} U_i}{m 4\pi\varepsilon_0} \sum_{j=-\infty, j\neq i}^{\infty} \frac{c_j U_j (z_i - z_j)}{r_{i,j}^3} \end{aligned}$$

Given the equilibrium $([z_e,\ 0]^T, U_e)$, we define $x_{i1} := z_i - z_e$, $x_{i2} := \dot{z}_i$, $x_{e1} := z_e$, $V_i := U_i - U_e$, and $V_e := U_e$. The linearized equation of motion for the above model in the state space form is given below:

$$\begin{aligned} \dot{x}_{i1} &= x_{i2} \\ \dot{x}_{i2} &= -bx_{i2} - x_{i1}\left(\omega^2 - \frac{\varepsilon_0 A V_e^2}{md^3}\right) + \left(\frac{2x_{e1}\varepsilon_0 A V_e}{md^3} + \frac{\varepsilon_0 A V_e}{md^2}\right) V_i \\ & - \left(1 + \frac{x_{e1}^2}{d^2} + \frac{2x_{e1}}{d}\right) \varepsilon_0 \frac{A^2 V_e^2}{d^2 m 4\pi} \sum_{j=-\infty, j\neq i}^{\infty} \frac{\delta x_{1ji}}{r_{i,j}^3} + \frac{1}{m} \sum_{j=i-1, j\neq i}^{j=i+1} \gamma_{i,j} \delta x_{1ji} \end{aligned}$$

Where $\delta x_{1ji} = x_{j1} - x_{i1}$. The current generated as a result of the excitation of microcantilevers is considered to be the output of the system and its expression is given as $y_i = \frac{d(c_i V_i)}{dt}$, Where, $c_i = \frac{\varepsilon_0 A}{(d - z_i)} = \frac{\varepsilon_0 A}{d}\left(1 + \frac{z_i}{d} + \left(\frac{z_i}{d}\right)^2 + \ldots\right)$ since $d > z_i$. Using first order approximation for c_i, we have

$$y_i = V_i \frac{\varepsilon_0 A}{d^2} x_{i2} + \frac{\varepsilon_0 A}{d} \dot{V}_i + \frac{\varepsilon_0 A x_{i1}}{d^2} \dot{V}_i$$

Linearizing the above equation around the equilibrium, we get,

$$y_i = \frac{V_e \varepsilon_0 A}{d^2} x_{i2} + \dot{V}_i \left(\frac{\varepsilon_0 A}{d} + \frac{\varepsilon_0 A x_{e1}}{d^2}\right)$$

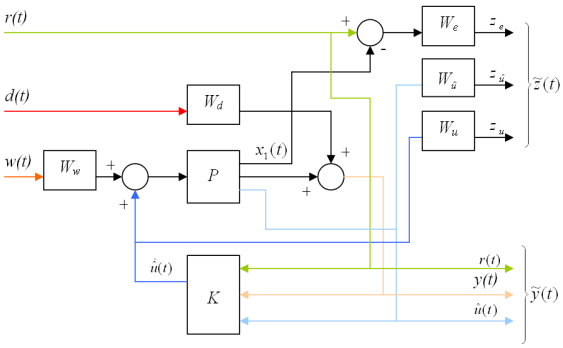

Fig. 2. Setup for LFT Formulation

C. Spatio-Temporal Scaling

We employ spatio-temporal scaling to improve the computational efficiency of the system. In doing so we define: $[\hat{x}_{i1}\ \hat{x}_{i2}]^T = \delta_x[x_{i1}\ x_{i2}]^T$, $\hat{y}_i = \delta_y y_i$, $\hat{V}_i = \delta_V V_i$, and $\tau = \omega_0 t$, where δ_x, δ_y, δ_V and ω_0 are scaling factors. We now define the following

$$\begin{aligned} a_{11} &= 0, \quad a_{12} = 1; \quad a_{22} = -\frac{b}{\omega_0} \\ a_{21} &= -\frac{\omega^2}{\omega_0^2} + \frac{\varepsilon_0 A \hat{V}_e^2}{\omega_0^2 m d^3 \delta_V^2} - \frac{1}{m\omega_0^2} \sum_{j=i-1, j\neq i}^{i+1} \gamma_{i,j} \\ &- \left(1 + \frac{\hat{x}_{e1}^2}{d^2\delta_x^2} + \frac{2\hat{x}_{e1}}{d\delta_x}\right) \varepsilon_0 \frac{A^2 \hat{V}_e^2}{d^2 m 4\pi\omega_0^2 \delta_V^2} \sum_{j=-\infty, j\neq i}^{\infty} \frac{1}{r_{i,j}^3} \end{aligned}$$

and

$$\hat{A} = \begin{bmatrix} a_{11} & a_{12} \\ a_{21} & a_{22} \end{bmatrix}; \quad \hat{B} = \begin{bmatrix} 0 \\ \frac{\delta_x}{\delta_V}\left(\frac{2\hat{x}_{e1}\varepsilon_0 A\hat{V}_e}{md^3\omega_0^2\delta_V^2} + \frac{\varepsilon_0 A\hat{V}_e}{md^2\omega_0^2}\right) \end{bmatrix}$$

$$\hat{G}_{i,j} = \sum_{j=-\infty, j\neq i}^{\infty} \begin{bmatrix} 0 & 0 \\ \frac{1}{m\omega_0^2}\gamma_{i,j} - \left(1 + \frac{\hat{x}_{e1}^2}{d^2\delta_x^2} + \frac{2\hat{x}_{e1}}{d\delta_x}\right)\varepsilon_0 \frac{A^2\hat{V}_e^2}{d^2 m 4\pi\omega_0^2\delta_V^2}\frac{1}{r_{i,j}^3} & 0 \end{bmatrix}$$

Where we have used the fact that $\gamma_{i,i+k} = 0$ for $|k| > 1$. Extending the state variables to include $\hat{x}_3 = \hat{V}$, the state space formulation is modified as follows;

$$\tilde{A} = \begin{bmatrix} \hat{A} & \hat{B} \\ 0 & 0 \end{bmatrix}; \tilde{B} = \begin{bmatrix} 0 \\ 0 \\ 1 \end{bmatrix}; \tilde{G}_{i,j} = \begin{bmatrix} \hat{G}_{i,j} & 0 \\ 0 & 0 \end{bmatrix};$$

$$\hat{C} = \begin{bmatrix} 0 & \frac{\hat{V}_e\varepsilon_0 A}{d^2} & 0 \end{bmatrix}; \hat{D} = \begin{bmatrix} \frac{\delta_x}{\delta_V}\omega_0\left(\frac{\varepsilon_0 A}{d} + \frac{\varepsilon_0 A\hat{x}_{e1}}{d^2}\right) \end{bmatrix}$$

The entire system can now compactly be written as for the i_{th} microcantilever

$$\begin{aligned} \dot{\hat{x}}_i &= \tilde{A}\hat{x}_i + \sum_{j=-\infty, j\neq i}^{\infty} \tilde{G}_{i,j}\hat{x}_j + \tilde{B}\dot{\hat{V}}_i \\ \hat{y}_i &= \tilde{C}\hat{x}_i + \tilde{D}\dot{\hat{V}}_i \end{aligned} \tag{4}$$

D. LFT Formulation

We define the following for the LFT setup shown in Figure 2. We define

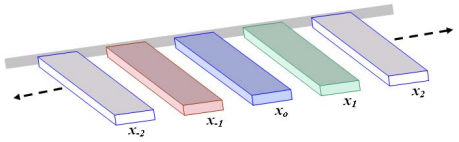

Fig. 3. Spatially Invariant Framework

$$\tilde{y} = \begin{bmatrix} \hat{y} \\ \hat{u} \\ r \end{bmatrix}; \tilde{z} = \begin{bmatrix} \tilde{r} - \tilde{x}_1 \\ \tilde{u} \\ \bar{u} \end{bmatrix}; \tilde{w} = \begin{bmatrix} \hat{w} \\ \hat{d} \\ r \end{bmatrix};$$

$\hat{u} = \hat{V}$ and $\tilde{u} = W_u\dot{\hat{V}}; \bar{u} = W_{\hat{u}}\hat{u}$, where W_u, and $W_{\hat{u}}$ are the design weights, and $\hat{w}$ is any external disturbance entering the system. $z_e = \tilde{r} - \tilde{x}_1 = W_e(r - x_1)$ is the weighted tracking error. W_u, and $W_{\hat{u}}$ are chosen so that the control effort does not exceed the allowable limit of $\pm 7.5V$ as per [5] and its rate of change remains reasonable. $W_{\hat{d}}$ is chosen such that the effect of high frequency measurement noise on the system output is attenuated. W_e is chosen to maximize the device bandwidth. We define bandwidth as the maximum excitation frequency where the tracking error remains less than or equal to $\pm 2nm$. W_w is chosen to attenuate the effect of any external disturbance entering the system at the input channel . For details see [16].

III. DISTRIBUTED CONTROLLER DESIGN

In this section we attempt to apply the recent results of distributed control [13] to our system, and analyze the robust performance [15] of the ensuing distributed controller.

A. Spatially-invariant Formulation

Let x_i in Figure 3 denote the state of the corresponding segment, i.e. $x_i = [x_{i1}, x_{i2}, x_{i3}]'$. Where x_{i1} is the position of the tip of microcantilever, x_{i2} is the velocity of the microcantilever tip, and x_{i3} is the applied voltage. Define the spatial shift operator S by $x_1 = Sx_0$, $x_{-1} = S^{-1}x_0$. The state of k_{th} microcantilever can be expressed in the form of $S^k x_0$, where $k \in \mathbb{Z}$. The dynamics of each segment are:

$$\begin{aligned} \dot{x}_i &= A(S)x_i + B_1 w_i + B_2 u_i \\ y_i &= Cx_i + Du_i + d_i \end{aligned} \tag{5}$$

where u_i is the rate of applied voltage, w_i captures any external disturbance effects such as moisture and wind effects on each element, and d_i is the noise in the output.The system dynamics in Equation (5) are entirely captured in $A(S)$, and its expression is given by: $A(S) = \sum_{j=-\infty}^{\infty} A_j S^j$ where for a given i, $A_0 = \tilde{A} - \sum_{j=-\infty, j\neq i}^{\infty} \tilde{G}_{i,j}$, and $A_j = \tilde{G}_{i,j}$ (see Equation (4)). What we seek here is a controller for each element that could use information from only finite number of its neighbors and meet the performance objectives without any significant loss.

When applying the $\mathscr{H}_\infty$distributed control methods of [13], we need to evaluate the spatial shift operator $S = e^{j\theta}$ over the

interval $[0,2\pi]$. Approximations of the state space matrices $A_c(S)$, $B_c(S)$, $C_c(S)$, and $D_c(S)$ for the distributed controller can be obtained by considering only a finite number of expressions in terms of the spatial operator S. Since the cantilevers are spatially-invariant, and symmetric, we approximate, say the state matrix $A_c(S)$ by the symmetric group of operators in S, and S^{-1}. For example, an approximation using only three neighbors on either side, which has seven terms, is as follows:

$$\begin{aligned} A_c(S) &= A_{c_{-3}}S^{-3}+A_{c_{-2}}S^{-2}+A_{c_{-1}}S^{-1}+A_{c_0} \\ &+ A_{c_1}S+A_{c_2}S^2+A_{c_3}S^3 \end{aligned} \tag{6}$$

The coefficient matrices A_{c_i} of the expansion can be determined using LSE [14].

The coefficient matrices A_{c_i} of the expansion can be determined using LSE [14]. To illustrate the procedure, we calculate the seven coefficient matrices in Equation (6). Let n denote the dimension of the matrix $A_c(S)$, and with slight abuse of notation, we use $A_c(k)$ to represent the value of the operator $A_c(S)$. Let m be the number of gridding points of Fourier frequencies θ, then $A_c(k)$ at the k_{th} gridding point of the Fourier frequency θ is

$$\begin{aligned} A_c(k) &= (I_n e^{-3j\theta_k}, I_n e^{-2j\theta_k}, I_n e^{-j\theta_k}, I_n, I_n e^{j\theta_k}, I_n e^{2j\theta_k}, I_n e^{3j\theta_k}) \\ &\quad \times (A_{c_{-3}}, A_{c_{-2}}, A_{c_{-1}}, A_{c_0}, A_{c_1}, A_{c_2}, A_{c_3})^* \\ &:= \psi_k \times \Omega \end{aligned} \tag{7}$$

where Ω is the real coefficient matrix of $(A_{c_{-3}}, \cdots, A_{c_0} \cdots A_{c_3})^*$, and $j = \sqrt{-1}$.

Since at each Fourier frequency point θ, the value of ψ_k is easily calculated and the matrix $A_c(S)$ is the state matrix of the controller, stacking all the Equations (7) at every gridding point, we get

$$\begin{pmatrix} A_c(1) \\ A_c(2) \\ \vdots \\ A_c(m) \end{pmatrix} = \begin{pmatrix} \psi_1 \\ \psi_2 \\ \vdots \\ \psi_m \end{pmatrix} \Omega \tag{8}$$

or

$$A_c = \Phi \times \Omega$$

Using LSE theorem in [14], one of the best coefficient matrix estimates is given by

$$\Omega = [(Re\,\Phi)'(Re\,\Phi)+(Im\,\Phi)'(Im\,\Phi)]^{-1} \begin{pmatrix} Re\,\Phi \\ Im\,\Phi \end{pmatrix}' \begin{pmatrix} Re\,A_c \\ Im\,A_c \end{pmatrix}.$$

where Re denotes the real part and Im denotes the imaginary part.

For better approximation of $A_c(S)$, higher order polynomials of S, S^{-1} can be used. The $\mathscr{H}_\infty$ controller is described as

$$\begin{aligned} \dot{x}_c &= A_c x_c + B_c y_c \\ u_c &= C_c x_c + D_c y_c. \end{aligned}$$

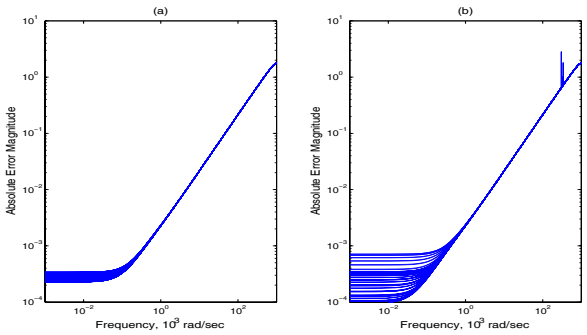

Fig. 4. Bode Magnitude Plot for Reference to Error Transfer Function Using (a) Information From 10,000 Neighbors and (b) and Using Only 2 Neighbors (1 on Each Side)

In the case of approximation (6), the structure of the controller is given as

$$\begin{aligned} \dot{x}_c &= [A_{c_{-3}}S^{-3}+\cdots+A_{c_0}+\cdots+A_{c_3}S^3]x_c \\ &\quad + [B_{c_{-3}}S^{-3}+\cdots+B_{c_0}+\cdots+B_{c_3}S^3]y_c \\ u_c &= [C_{c_{-3}}S^{-3}+\cdots+C_{c_0}+\cdots+C_{c_3}S^3]x_c \\ &\quad + [D_{c_{-3}}S^{-3}+\cdots+D_{c_0}+\cdots+D_{c_3}S^3]y_c \end{aligned}$$

which means that to calculate the local control, each controller needs to communicate with six cantilevers and controllers in its immediate neighborhood (three on either side). Simulations of the linear system with the distributed controller suggest that a maximum bandwidth of 9,400 rad/sec can be achieved before utilizing excessive control effort. In the nonlinear system, however, a resonance like phenomenon is experienced when excited beyond a frequency level of 3,000 rad/sec. For details see [16].

B. Controller Spatial Truncation

Figure 4(a) shows Bode magnitude plot, at different gridding points of the Fourier frequency θ, for reference to error transfer function when the controller uses information from its 10,000 neighbors (5,000 on each side).

The localization of the coupling effects on the i_{th} microcantilever permits the use of information from the immediate neighbors only yet delivering performance that is comparable to the full information controller. The Bode magnitude plot of the reference to error transfer function at various Fourier frequencies θ for this case is shown in Figure 4(b). Notice that the system does not suffer any loss of bandwidth as compared to the case in Figure 4(b) discussed above.

C. Simulation of Nonlinear Model

We simulate the truncated controller on a 10-segment nonlinear system of microcantilever array. Each controller was in communication with only its immediate neighbors and was also receiving information for the system output (current measured) from its neighboring cantilevers except

for the controllers at the edge of the array. The controllers at the edge were truncated such that no information was passed to them from their neighbors. Asymmetric truncation of the controllers at the edge was seen to cause destabilization. The reference input was fixed at a frequency of 3,000 rad/sec, with a magnitude of about 10nm with different (and independent) phase shifts. The resulting absolute tracking error plots are presented in Figure 5. The performance of the edge cantilevers and their immediate neighbors is seen to degrade since the lack of information at the edge cantilevers results in tracking error propagation to their immediate neighbors. This tracking error propagation is, however, localized. This is evident from the fact that an absolute error bound of 1.75nm is observed at the non-immediate neighbors of the edge cantilevers as opposed to 5nm, and 25nm which is observed for the immediate neighbors of the edge cantilevers and the edge cantilevers respectively. This resolution is comparable to what is achieved when a centralized controller is employed for a system of eight microcantilever array as shown in Figure 6.

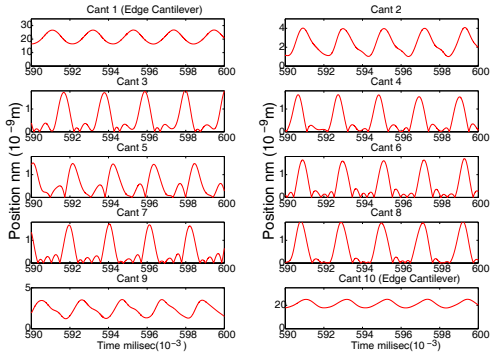

Fig. 5. Tracking Error For the Array System of Ten Cantilevers at Same Excitation Frequency (3,000 rad/sec) Using Truncated Controller

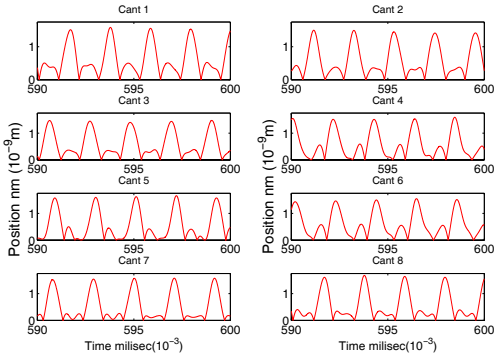

Fig. 6. Tracking Error For the System of Eight Cantilevers at Same Excitation Frequency (3,000 rad/sec) While Employing a Centralized Controller

IV. Robustness Analysis

The theory regarding the system robustness of distributed systems can be found in [15]. We consider only the effects of parametric uncertainty in system of multicantilever array in order to get an idea of the sensitivity of the baseline design. We, therefore, develop herein an uncertainty model to be analyzed. The lumped system parameters (as presented in Section II) were assumed to have some degree of uncertainty as expressed below. Define:

$$a_{21}(\theta) := \frac{\omega_e^2}{\omega_0^2} + \frac{\varepsilon_0 A \hat{V}_e^2}{\omega_0^2 m d^3 \delta_V^2} + \frac{1}{m\omega_0^2} \sum_{m=l-1, m\neq l}^{l+1} \gamma_{l,m}\left(e^{jm\theta}-1\right)$$

$$-\left(1+\frac{\hat{x}_{e1}^2}{d^2\delta_x^2}+\frac{2\hat{x}_{e1}}{d\delta_x}\right)\varepsilon_0\frac{A^2\hat{V}_e^2}{d^2 m 4\pi\omega_0^2\delta_V^2}\sum_{m=-\infty, m\neq l}^{\infty}\frac{1}{r_{l,m}^3}\left(e^{jm\theta}-1\right)$$

$$a_{22} := \frac{b}{\omega_0}; \qquad a_{23} := \frac{\delta_x}{\delta_V}\left(\frac{2\hat{x}_{e1}\varepsilon_0 A\hat{V}_e}{md^3\omega_0^2\delta_V^2}+\frac{\varepsilon_0 A\hat{V}_e}{md^2\omega_0^2}\right)$$

$$c_{62} := \frac{\hat{V}_e\varepsilon_0 A}{d^2}; \qquad d_{64} := \frac{\delta_x}{\delta_V}\omega_0\left(\frac{\varepsilon_0 A}{d}+\frac{\varepsilon_0 A\hat{x}_{e1}}{d^2}\right)$$

$$\overline{a_{21}(\theta)} := a_{21}(\theta)(1+\alpha_2\delta_2); \qquad \overline{a_{22}} := a_{22}(1+\alpha_1\delta_1)$$
$$\overline{a_{23}} := a_{23}(1+\alpha_3\delta_3); \qquad \overline{c_{62}} := c_{62}(1+\alpha_4\delta_4)$$
$$\overline{d_{64}} := d_{64}(1+\alpha_5\delta_5)$$

Where $\overline{(\cdot)}$ is the perturbed lumped parameter, and $(\cdot)$ is the nominal value of the lumped parameter. $\alpha_i \in \mathbb{R}$ is the percentage uncertainty of the given parameter and $\delta_i \in \mathbb{C}$ is the size of uncertainty the system can tolerate with a reasonable bound on the allowable tracking error. We focus mainly on the transfer function from $\tilde{w} \rightarrow e$ (where e is the tracking error) in developing the framework for the uncertainty analysis. The μ plot of the system as shown in Figure 7 permits a 0.44% uncertainty margin for $a_{21}(\theta)$ and a_{23}, while rest of the lumped parameters admit an allowance of 40%. Random perturbations of varying size

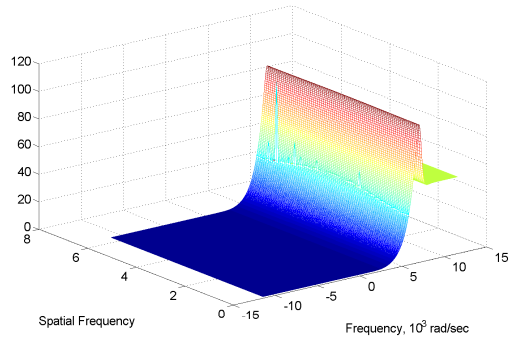

Fig. 7. Structure Singular Value Plot For Robust Performance

were introduced. The operation of an array of ten such randomly perturbed linear models of microcantilevers was simulated. The allowable uncertainty bounds on a_{21} and a_{23} as established above, were found to be quite conservative as the system was found to tolerate an uncertainty margin of up

to 11% on these parameters. This is in line with the fact that the μ analysis is a worst-case analysis and these margins leave a high degree of conservatism. The reference input was fixed at a frequency of 3,000 rad/sec, with a magnitude of about 10nm. The absolute tracking error plot for the perturbed linear system is shown in Figure 8. The error plot is seen to be within a bound of 1.75nm. Also, random perturbations of varying size in the parameters of natural frequency and the damping coefficient were introduced in the nominal nonlinear model of the microcantilevers. An array consisting of ten such randomly perturbed nonlinear models of the microcantilever system was simulated. It was found that the designed controller could admit 10% perturbation in the parameter of natural frequency, whereas the damping coefficient could admit 40% perturbation given that the frequency of excitation does not exceed a level of 2,500 rad/sec.

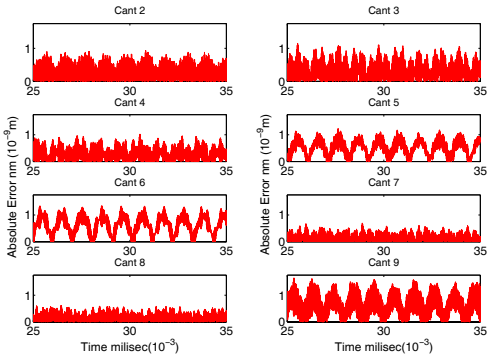

Fig. 8. Absolute Tracking Error Plot For The Perturbed Linear System Simulated at 3,000 rad/sec (Only Non-edge Cantilevers Shown)

V. CONCLUSION

We presented a model of an infinite array of electrostatically actuated microcantilevers and a baseline control design. The desired performance levels characterized by a bandwidth of 3,000 rad/sec and a resolution of 1.75nm can be met by employing a centralized controller on a finite system (not presented here, for details see [16]). The implementation of this approach, however, becomes increasingly complicated as the order of the given system increases. A centralized controller with an order forty is required for a system of eight cantilevers in order to fulfill the task. We have shown that for the given system of microcantilevers, a distributed controller with a localized architecture (with order five) can delivers a performance level comparable to a centralized controller. The performance of edge cantilevers and their immediate neighbors was seen to deteriorate for a finite system, while rest of the system met the performance specifications. From an operational point of view, the use of the edge cantilevers and their immediate neighbors can be abandoned while making use of the rest. We have also demonstrated that the designed controller brings a certain degree of robustness with it. The achieved bandwidth of the device allows it to be used in the "contact mode" of operation in regular AFMs, in addition for its employment for various nano-positioning mechanical tasks like indenting, pushing, cutting, lithography etc. We have, hence, provided a feasible solution to tackle the dynamical coupling effect of the proposed device without compromising the compactness of its size.

VI. ACKNOWLEDGMENTS

This research is supported in part by NSF Award CMS0301516 and AFOSR Grant FA9950-06-1-0252.

REFERENCES

[1] B.W. Chui et al., "Independent Detection of Vertical and Lateral Forces with Sidewall-Implanted Dual-axis Piezoresistive Cantilever" *Appl. Phys. Lett.*, Vol. 72, No.11, pp.1388-1390, March 1998

[2] M. Tortonese et al., "Atomic Resolution with an Atomic Force Microscope Using Piezoresistive Detection", *Appl. Phys. Lett.*, Vol. 62, pp.834-836, March 1993

[3] Gaucher et al., "Piezoelectric Bimorph Cantilever for Actuation and Sensing Applications", *J. Phys. IV France*, Vol. 8, pp.235-238, March 1998

[4] T. Itoh, et al., "Piezoelectric cantilever Array for Multiprobe Scanning Force Microscopy", *Proc. of the IX int. Workshop on MEMS, San Diego, CA, USA*, 11-15 Feb. 1996. New York, NY USA: IEEE, 1996. PP. 451-455

[5] M. Napoli, B.Bamieh and K.Turner., "A Capacitive Microcantilever : Modeling, Validation and Estimation Using Current Measurements", *ASME Journal of Dynamic Systems Measurement and Control*, Volume 126, Pages 319-326, June 2004

[6] S.C. Minne et al., "Parallel Atomic force Microscopy Using Cantilevers with Integrated Piezoresistive Sensors and Integrated Piezoelectric Actuators", *Appl. Phys. Lett.*, Vol. 67, No 26, pp. 3918-3920, 1995.

[7] Q.A. Huang et al., "A simple Approach to Characterizing the Driving Force of Polysilicon Laterally Driven Thermal Micro Actuators", *Sensors and Actuators*, 80, pp. 267-272, 2000

[8] P. Attia et al., "Fabrication and Characterization of Electrostatically Driven Silicon Microbeams", *Microelectronics J.*, 29, pp. 641-644, 1998

[9] N. Blanc et al., "Scanning Force Microscopy in Dynamic Mode Using Microfabricated Capacitive Sensors", *J. Vac. Sci. Technol. B*, 14(2), pp. 901-905, Mar/Apr 1996

[10] M. Napoli et al., "Dynamics of Mechanically and Electrostatically Coupled Microcantilevers", *in Proc. Of Transducers03*, Boston MA, 2003

[11] M. Napoli et al., "Modeling, validation and estimation for capacitively actuated microcantilevers with current measurements", *ASME Journal of Dynamic Systems, Measurement, and Control*, 2004

[12] M. Napoli et al., "Design of a Decoupling Controller for Electrostatically Coupled Microcantilevers Based on Current", *In Proc. Of 2004 ACC Boston MA*, June 30th July 2, 2004

[13] Bamieh, B.F. Paganini and M. A. Dahleh, "Distributed Control of Spatially Invariant Systems", *IEEE Transactions on Automatic Control*, Vol. 47, No. 7, pp.1091-1107. 2002.

[14] Ljung, L, "System Identification: Theory for the User", Prentice Hall, Inc. 1987.

[15] Dimitry Gorinevsky and Gunter Stein, "Structured Uncertainty Analysis of Robust Stability for Multidimensional Array System", *IEEE Transaction on Automatic Control*, Vol. 48, pp. 1557-1568. 2003.

[16] Azeem Sarwar, "Modeling and Control of Electrostatically Actuated Microcantilever Array", MS Thesis, University of Illinois Urbana Champaign, Department of Mechanical and Science Engineering, Oct 2006.